nature chemistry

ARTICLES

PUBLISHED ONLINE: 18 MARCH 2012 | DOI: 10.1038/NCHEM.1298

Ionization of dimethyluracil dimers leads to facile proton transfer in the absence of hydrogen bonds

Amir Golan[1,4], Ksenia B. Bravaya[2], Romas Kudirka[3], Oleg Kostko[1], Stephen R. Leone[1,4], Anna I. Krylov[2]* and Musahid Ahmed[1]*

Proton transfer is ubiquitous in chemistry and biology, occurring, for example, in proteins, enzyme reactions and across proton channels and pumps. However, it has always been described in the context of hydrogen-bonding networks ('proton wires') acting as proton conduits. Here, we report efficient intramolecular ionization-induced proton transfer across a 1,3-dimethyluracil dimer, a model π-stacked system with no hydrogen bonds. Upon photoionization by tunable vacuum ultraviolet synchrotron radiation, the dimethyluracil dimer undergoes proton transfer and dissociates to produce a protonated monomer. Deuterated dimethyluracil experiments confirm that proton transfer occurs from the methyl groups and not from the aromatic C–H sites. Calculations reveal qualitative differences between the proton transfer reaction coordinate in the π-stacked and hydrogen-bonded base pairs, and that proton transfer in methylated dimers involves significant rearrangements of the two fragments, facilitating a relatively low potential energy barrier of only 0.6 eV in the ionized dimer.

Proton transfer is ubiquitous in chemistry and biology (for example, in proteins, enzymes, proton channels and proton pumps), but has always been described in the context of hydrogen-bonding networks acting as proton wires. Some important examples include excited-state proton transfer between nucleobases, which provides an efficient energy relaxation pathway[1] and contributes to the intrinsic photostability of DNA. In oxidized DNA, proton transfer separates the unpaired electron and positive charge between the two strands, thus terminating long-range hole migration[2]. Excited-state proton transfer is also a key step in the photocycle of green fluorescent protein[3]. Indeed, some of the most important biochemical pathways in life itself are arguably proton transfers across proteins and through membranes[4,5].

The mechanism of proton transfer has always involved hydrogen-bonded networks acting as proton conduits[6–8], and proton transfer between Watson–Crick pairs induced by photoexcitation and/or photoionization of nucleobases[9,10] is not an exception. This Article presents evidence for (and quantifies) proton transfer in the absence of hydrogen bonds across π-stacked dimers of ionized nucleobases. It allows us to speculate that novel proton transfer pathways, such as along π-stacked arrays and non-conventional hydrogen bonds[11] (that is, C–H···O and N–H···O), may be operational in various biological processes, including molecular recognition and folding of RNA and DNA[12], as well as carbohydrate–protein interactions[13]. We also speculate that, because hydrocarbons on surfaces often assume π-stacked geometries, proton transfer through π-stacks could have implications for catalysis[14]. These findings might also have relevance in environmental chemistry, because π-stacking is present in soil and sediments, and it might be anticipated that these proton-transfer pathways might affect the rates of absorption of various molecules and ions at organic interfaces[5].

π-Stacking motifs are common in biochemical systems such as DNA, lipid bilayers and melanin pigments, in DNA contributing to the structural integrity of the DNA double helix and playing an important role in radiation- or ionization-induced processes[16–18] such as hole migration along the DNA strands[5] and the formation of excimers, oxidized products and fused dimers[17–19]. In synthetic lipid bilayers, the rigidity conferred by π-stacking architectures has led to novel applications for artificial photosystems by forming ion channels and supramolecular rosettes[18–21]. Melanin[22], the structure of which is believed to be dominated by π-stacking[23], protects living systems from UV radiation by conferring colour to them, and the mechanism of photoprotection may involve excited-state proton transfer (PT)[24], by analogy with DNA (ref. 1). Quantum mechanics explains the effects of π-stacking on electronically excited or ionized states in terms of efficient molecular orbital overlap facilitating the delocalization of the excitation (or electron hole) over stacked systems. However, the π-stacking arrangement is not optimal for proton transfer. A crucial question for such systems is 'How does a proton find a transfer path in the absence of a guiding hydrogen-bonding network?'.

Proton transfer in nucleobases has been investigated in liquid[25,26] and gas-phase dimers[27–29] and is identified as one of the relaxation pathways of ionized nucleobase dimers[30–33]. These previous studies reveal that the photoionization relaxation patterns are different for π-stacked and hydrogen-bonded dimers. In the former, ionization may result in the formation of fused dimers with partially covalent bonding between the monomers and bonding energies of $\sim$20 kcal mol^{-1}. In the latter, hydrogen-bonded dimers (AA, TT, AT, CC, GC), ionization leads to efficient proton transfer. The resulting dimers are bound by 30–35 kcal mol^{-1}. Ground-state proton transfer between bases is endothermic (for example, by 0.75 eV in AT), but in the ionized states it is exothermic by 0.4–0.8 eV (Supplementary Section S3). Hence, when sufficient energy is available to the ionized dimers, they dissociate to produce protonated species.

Uracil is chosen here because it has no low-energy tautomers to complicate interpretation of the experimental results[34], and there is robust theory regarding the ionization energetics of hydrogen-bonded and stacked pairs[30–32]. In this Article, we show that uracil

[1]Chemical Sciences Division, Lawrence Berkeley National Laboratory, Berkeley, California 94720, USA, [2]Department of Chemistry, University of Southern California, Los Angeles, California 90089-0482, USA, [3]Materials Sciences Division, Lawrence Berkeley National Laboratory, Berkeley, California 94720, USA, [4]Departments of Chemistry and Physics, University of California, Berkeley, California 94720, USA. *e-mail: krylov@usc.edu; mahmed@lbl.gov

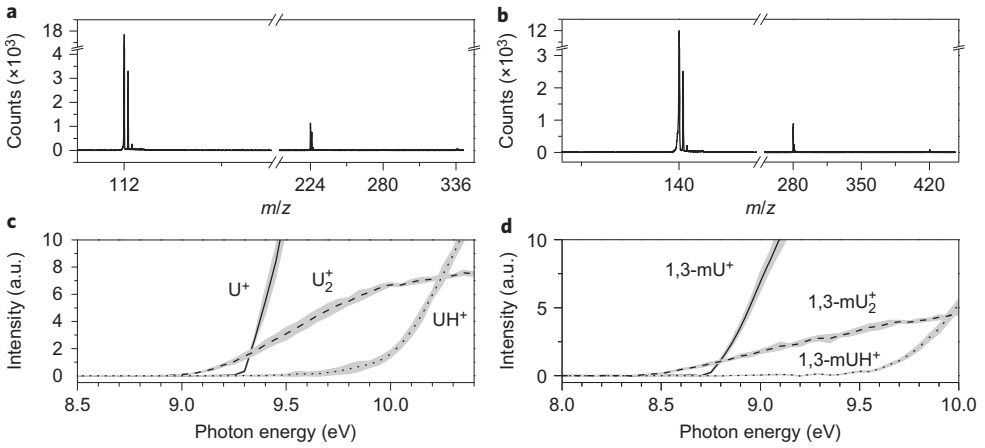

Figure 1 | VUV-SPI mass spectra and photoionization efficiency curves. a–d, Typical mass spectra and photoionization efficiency curves for uracil (**a**,**c**) and 1,3-mU (**b**,**d**) molecular beams. The signal at $m/z = 112$ corresponds to U^+, and the small peak at 113 is due to UH^+ (in addition to a 5.2% isotopic contribution). The peaks at $m/z = 140$ and 141 correspond to 1,3-mU^+ and 1,3-mUH^+, respectively. The lines (solid, dashed and dotted) denote the average of the experimental data. The standard deviation is shown as a grey area.

dimers follow the behaviour of other pyrimidine pairs, forming protonated monomers upon ionization. The observed ionization appearance energies are supported by calculated ionization energies for hydrogen-bonded and π-stacked dimers. In contrast to the barrierless and one-dimensional reaction coordinate for proton transfer in the uracil dimer, for 1,3-dimethyluracil (1,3-mU) dimers our calculations show a 0.6 eV barrier and a complex reaction coordinate involving significant rearrangements of the two mU moieties. The calculations support the experimentally observed large yield of protonated monomers upon ionization. To reveal the origin of the transferred proton, we investigated d6-1,3-dimethyluracil (d6-1,3-mU), in which the two methyl groups are deuterated and the C–H moieties on the ring are not. This allows us to distinguish whether the proton transfer involves the methyl group or the uracil ring. We observed that deuterium transfer, followed by dissociation of the dimer into the $(d6\text{-}1,3\text{-}mUD)^+$ ion and the presumed deprotonated radical, is the dominant reaction channel, with up to 69% of the ionized dimers following this channel and the other 31% remaining as ionized dimers. This confirms that the transfer originates from the methyl group and not from the aromatic C–H sites. This observation of facile ionization-induced proton transfer reveals the importance of the previously neglected proton transfer mechanisms in systems with no hydrogen bonds, such as methylated nucleobases, or with non-conventional hydrogen bonds. In the context of mass spectrometry, this reaction can be described as an interesting case of so-called 'chemical ionization', which was observed in methane in the 1960s and was used to softly ionize neutral species with a higher proton affinity[35]. The thermochemistry of this ion-neutral reaction involving proton transfer depends on the proton affinity of the reagents, and indeed Gronert and colleagues[36] measured the proton affinity of 1,3-mU in the gas phase to be 9.27 ± 0.13 eV and predicted that protonation takes place on the carbonyl groups. This high value offsets the energy penalty for breaking the C–H bond in the ionized 1,3-mU (~9.4 eV), resulting in a relatively small (negative) reaction enthalpy for proton transfer between the neutral and ionized monomers.

Results and discussion

Vacuum ultraviolet single photon ionization (VUV-SPI) mass spectrum of uracil and mU. A VUV-SPI mass spectrum of the uracil molecular beam features signals corresponding to U^+, U_2^+ and UH^+, and less than 3% of larger clusters (Fig. 1a). The mass spectrum of 1,3-mU follows the same pattern (Fig. 1b). Figure 1c shows the photoionization efficiency curves for the monomer, dimer and protonated monomers for uracil and 1,3-mU generated by integrating the area of each mass spectral peak at different photon energies. The observed onsets of the photoionization efficiency curves of U^+, U_2^+, 1,3-mU^+ and 1,3-mU_2^+ correspond to the calculated adiabatic ionization energies (Supplementary Table S1). In the uracil beam, the UH^+ channel exhibits a sharp rise at ~9.8 eV (Fig. 1c). Following ionization of the methylated sample, the π-stacked dimer shows a significant signal for 1,3-mUH^+ (protonated 1,3-dimethyluracil ion) with an onset at ~9.35 eV, demonstrating that proton transfer is efficient in the methylated species despite the absence of hydrogen bonds in the neutral dimer.

We consider the following channels giving rise to the observed ion signals, where M is the investigated molecule (one monomer unit):

$$M + h\nu \rightarrow M^+ \quad (1)$$

$$M_2 + h\nu \rightarrow \begin{cases} M_2^+ & (2) \\ MH^+ + (M - H) & (3) \\ M^+ + M & (4) \end{cases}$$

No other channels of dissociative ionization are detected in the mass spectra, in agreement with previous studies[37]. Larger clusters and microhydrated species due to traces of water present in the argon carrier gas will not give rise to the protonated monomer signal for a number of reasons. For d6-1,3-mU, no protonated monomers are observed; there is no notable signal for a sample + water complex or higher uracil clusters. On varying the backing pressure of the carrier gas, different amounts of dimers and trimers are detected in the supersonic molecular beam and there is no concomitant change in the protonated monomer signal. The latter observation suggests that the presence of trimers in the beam is negligible and that the beam mainly comprises monomers and dimers.

Furthermore, the effusive source signal shows no evidence of dimer or higher clusters and there is little change (less than 5%) in the photoionization efficiency curve shape of the monomer signal U^+ (or 1,3-mU^+) compared to those formed in the molecular beam. This would suggest that dimer dissociation, channel (4), contributes less than 5% to the ion signal. With this in mind, only the first three channels, (1) to (3), need to be considered to explain the experimental results.

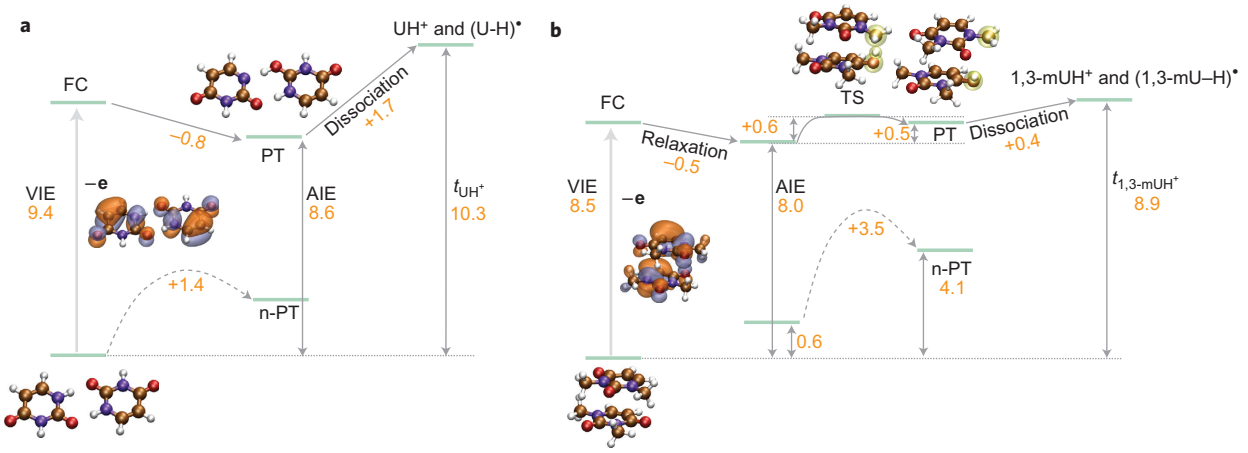

Figure 2 | Relevant computed energetics (eV) of the non-methylated hydrogen-bonded and methylated uracil dimers. a,**b**, Ionization and proton transfer energies are given for the lowest-energy U_2 (**a**) and 1,3-mU_2 (**b**) dimers. The shape of the initial hole corresponding to the lowest ionized state is also shown (see molecular orbitals). Upon ionization, U_2^+ relaxes to the proton transfer structure bound by 1.7 eV. In 1,3-mU_2^+, the Franck–Condon relaxed structure, which resembles a fused dimer (yellow spheres show the reaction moieties), is separated from the proton transfer structure by a barrier (transition state, TS). The dissociation energy of the proton transfer structure is 0.4 eV and threshold energies (t) for the formation of protonated monomers for the lowest-energy dimers of uracil and 1,3-mU are indicated by t_{UH^+} and $t_{1,3\text{-mUH}^+}$, respectively. n-PT refers to the proton transfer structure in the neutral dimer. AIE, adiabatic ionization energy. All energies except the vertical ionization energy (VIE) include zero point vibrational energy correction.

Ionization and proton transfer energetics. The energetics of channels (2) and (3) for the two representative systems[28,29] (lowest-energy U_2 and 1,3-mU_2) are illustrated in Fig. 2. The diagrams show the calculated adiabatic ionization energies that correspond to the photoionization efficiency onsets of the respective species (provided that the Franck–Condon factors are favourable) and thermodynamic onsets corresponding to the dissociation channel leading to formation of the protonated monomer. The observed photoionization efficiency onsets for U^+ and 1,3-mU^+ agree within 0.1 eV with the respective computed adiabatic ionization energies (see Supplementary Table S1). The experimental onsets of dimer photoionization efficiency and protonated monomer appearance signals can also be compared to the adiabatic ionization energies and threshold energies (t) for the formation of protonated monomers for the lowest-energy dimers of U and 1,3-mU (t_{UH^+} and $t_{1,3\text{-mUH}^+}$, respectively, in Fig. 2), with a caveat that the presence of other conformers in the molecular beam may lead to discrepancies between the apparent onsets and those computed for the most stable species.

The most stable conformer of U_2 is a symmetric hydrogen-bonded structure (Fig. 2a) bound by 0.70 eV (D_0). Higher in energy are several non-symmetric hydrogen-bonded structures followed by a π-stacked manifold that begins at ~0.4 eV above the lowest hydrogen-bonded conformer[30,38] (the binding energy of the most stable π-stacked conformer is 0.33 eV (D_0)). The hydrogen bond is rather conspicuous in the uracil dimer. The distance between the participating hydrogen and the oxygen of the complementary moiety is 1.76 Å, and the respective N–H bond length changes by 0.02 Å relative to the monomer. Most importantly, the system is poised for proton transfer due to the nearly collinear arrangement of the three participating atoms (the value of the NHO angle is 177°).

Methylation eliminates the hydrogen-bonded manifold completely. The lowest-energy conformer of 1,3-mU_2 is a π-stacked one (Fig. 2b, Supplementary Figs S7 and S8) and is bound by 0.57 eV (D_0). The equilibrium distance between the 1,3-mU in the gas-phase dimer is 3.30 Å, which is similar to the 3.33 Å separation between the bases in the DNA double helix. In addition to blocking the usual hydrogen-bonding interactions[29,38,39], methylation increases the electron density in the π-system, which decreases the ionization energies and modulates the strength of π-stacking interactions[22,31,40].

Calculations predict that proton transfer from methyl groups is more favourable energetically than proton transfer from the aromatic ring. To verify this experimentally we used deuterated 1,3-mU, in which the CH_3 groups were replaced by CD_3 and the CH groups were left intact (d6-1,3-mU). The mass spectrum of 1,3-mU shows the monomer signal and a smaller protonated monomer peak (Fig. 3a), but the d6-1,3-mU sample has three peaks, the first two corresponding to d6-1,3-mU^+ (at $m/z = 146$) and the deuterium-transferred form (d6-1,3-mUD)$^+$ ($m/z = 148$), respectively, and third being a small peak at $m/z = 147$. In Fig. 3b, trace (i) shows the ratio between protonated and unprotonated 1,3-mU signals, trace (ii) the ratio between the deuterium-transferred and bare monomers (d6-1,3-mUD^+/d6-1,3-mU), which is almost identical to the analogous 1,3-mU curve shown in trace (i). The traces in Fig. 3b begin with a constant background (~0.072 and 0, respectively) due to the natural abundance of C_{13} and N_{15} isotopes. They then rise sharply at ~9.6 eV, with a small shallow slope beginning at ~9.35 eV, indicating the onset for proton transfer. The ratio between $m/z = 147$ and 146 is photon-energy-independent, indicating that the $m/z = 147$ peak arises only from the isotope contribution and not hydrogen transfer (Fig. 3b, trace (iii)).

To establish the relationship between the apparent onsets for proton transfer and the underlying mechanism, we considered the energetics of the ionization-induced intramolecular proton transfer in nucleobase dimers, the first step leading to formation of the protonated monomers. In U_2, proton transfer is exothermic and barrierless in the ionized state. Methylation results in a significant barrier (0.6 eV) for proton transfer in ionized 1,3-mU_2. The structure after proton transfer is 0.5 eV higher in energy than the relaxed non-proton transferred structure and is isoenergetic with the vertical Franck–Condon geometry. The thermodynamic onsets for the formation of protonated monomers are computed as the energy difference between the initial neutral dimer and the products, UH^+ and (U–H)· (or 1,3-mUH^+ and (1,3-mU–H)·). For the lowest-energy dimers of U_2 and 1,3-mU_2, the proton transfer channel opens at 10.25 eV and 8.93 eV, respectively. Note that the shift in the thermodynamic onset for the d6-1,3-mUD^+ due to the difference in zero point energy (ZPE) is only 0.02 eV and the resulting threshold energy is 8.95 eV. Importantly, for both UH^+ and 1,3-mUH^+ systems, the thermodynamic onsets should

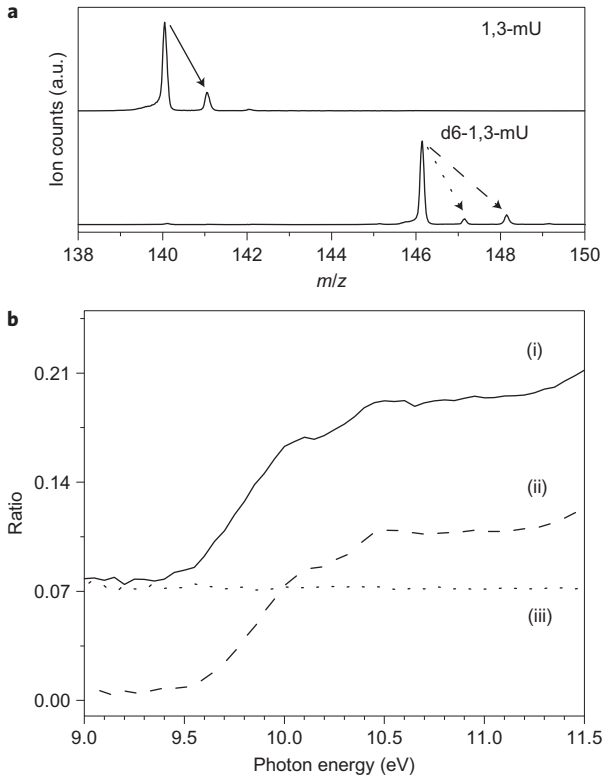

Figure 3 | Effect of deuteration on the 1,3-mU mass spectrum and photoionization efficiency curves. a, Mass spectra obtained at 10.50 eV for 1,3-mU and d6-1,3-mU zoomed in to show the monomer and protonated/deuterated peaks. (Arrows refer to ratios between peaks, shown in **b**.) **b**, Trace (i): ratio between the 1,3-mU$^+$ signal and (1,3-mUH)$^+$ ($m/z = 140$ divided by $m/z = 141$). Following the natural isotope background of 0.072% arising from the 0.0107% and 0.368% contributions of C_{13} and N_{15}, respectively, is the proton transfer onset at 9.35 eV. Traces (ii) and (iii): ratios between the monomer signal at $m/z = 146$ and the peaks at $m/z = 148$ and 147, respectively. Trace (ii) exhibits the same energy dependence as trace (i), but trace (iii) remains constant, demonstrating that no (observable) hydrogen is transferred from the C–H groups on the aromatic ring.

correspond to the appearance curve onsets, because there is no barrier for proton transfer in ionized hydrogen-bonded U_2 and the transition state energy is below the thermodynamic onset in 1,3-mU_2. If higher-energy conformers are present in the beam, the apparent onsets will be lowered. The binding energy of the lowest-energy dimer conformer ($D_0 = 0.57$ eV) also defines the uppermost energetically possible 1,3-mU_2 dimer. Hence, the most conservative estimate of the lower bound of the proton transfer channel onset for 1,3-mU_2 is 8.36 eV. This requires population of conformers that are 0.57 eV above the lowest one, rather unlikely even assuming non-Boltzmann distributions in the thermal desorption sources used. A similar estimate provides 9.10 eV as the lower bound energy for the proton transfer channel onset for U_2. Therefore, theory predicts that proton transfer channels should be accessible above 9.10 eV and 8.36 eV for uracil and 1,3-mU, respectively, and that the signal from the lowest-energy dimer starts to contribute at 10.25 eV and 8.93 eV, respectively. Indeed, the observed experimental onsets for UH^+ and 1,3-mUH^+ signals lie above the predicted lower bound of the proton transfer channel onsets, possibly as a result of unfavourable Franck–Condon factors and population of higher-energy conformers of the dimers in the molecular beam. For UH^+, the sharp rise of the signal at 9.8 eV is in excellent agreement with the values predicted for two higher-energy hydrogen-bonded dimers of U_2 (Supplementary Fig. S12). In summary, the observed onsets of the appearance of protonated uracil and 1,3-mU are within the theoretically predicted bounds, and the sharp UH^+ signal rise correlates with the theoretical values of the most abundant conformers.

Branching ratios and deuteration effects. To obtain detailed information about the proton transfer channel, we analysed the branching ratios between the proton transfer and formation of the ionized dimer. The contribution of dimer dissociation to the monomer signal, channel (4), is not substantial, so ionized dimers give rise to only U_2^+ or UH^+ signals (1,3-mU_2^+ and 1,3-mUH^+ in the methylated species). Consequently, the branching ratio for the proton transfer channel is given by

$$\frac{MH^+}{M_2^+ + MH^+} \qquad (5)$$

where MH^+ and M_2^+ are the photoionization efficiency signals of the protonated monomer and the dimer, respectively. These ratios for uracil, 1,3-mU and d6-1,3-mU are shown in Fig. 4. These ratios characterize the efficiency of the proton transfer channels in different species.

Asymptotically, the efficiency of proton transfer in uracil and dimethyluracil is remarkably similar and approaches an 85% fraction of the ionized dimers for uracil and 1,3-mU. The deuterated curve lags behind the non-deuterated signal and approaches a lower asymptotic value of 69% (the remaining 31% do not fragment and remain as ionized dimers). Similar values derived from a Rice–Ramsperger–Kassel–Marcus (RRKM) model are in semi-quantitative agreement with the experiment results, 75% and 67% for 1,3-mUH^+ and d6-1,3-mUD^+, respectively (Supplementary Section S6). The small effect of H/D substitution on the observed yield of protonated monomers points to the complex reaction coordinate for the proton transfer process. The presence of different conformers in the molecular beam, and the possible involvement of multiple ionized states with different ionization cross-sections, potential energy surfaces and anharmonic effects, make quantitative predictions of kinetic isotope effects extremely difficult in these systems.

Proton transfer mechanism. The nature of motions promoting low-energy proton transfer in the ionized state is very different for

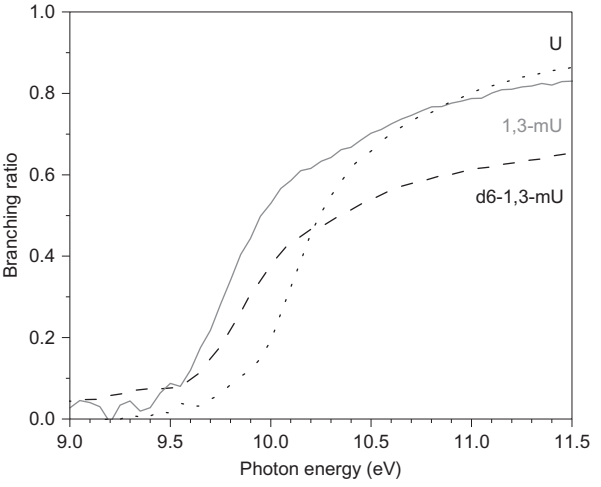

Figure 4 | Experimental branching ratios for the proton transfer channel in the uracil, 1,3-mU and d6-1,3-mU beams. Although showing different onsets, the proton transfer efficiencies in uracil and dimethyluracil are remarkably similar, reaching 85%. The deuterated curve lags behind the non-deuterated signal and approaches a lower asymptotic value of 69%.

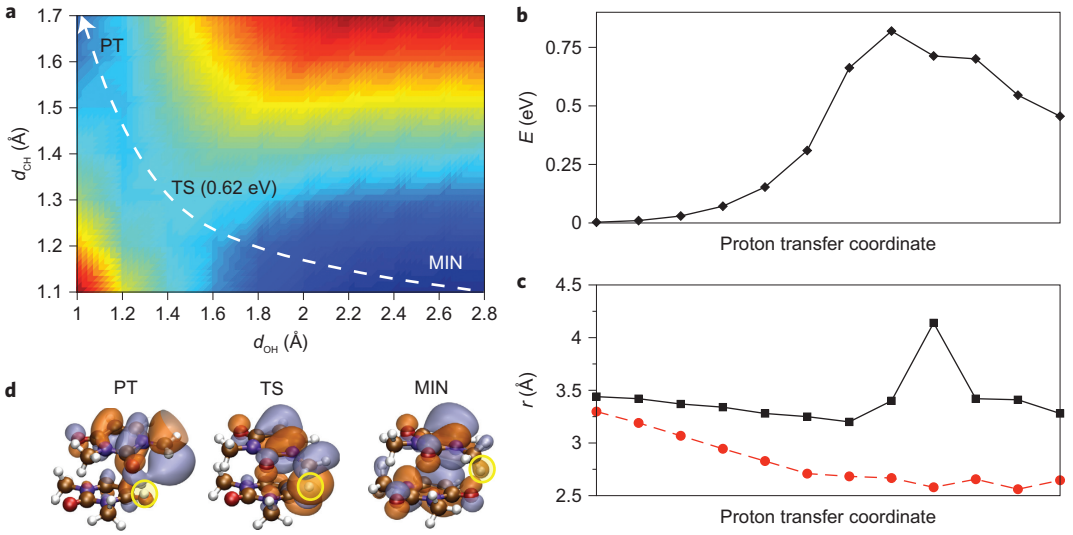

Figure 5 | Relevant energetic and structural parameters illustrating the mechanism of ionization-induced proton transfer. a, The two-dimensional PES scan shows the proton transfer path in the dimer ion (1,3-mU_2^+) involving a concerted change in the distances between the proton and the donating (C–H) and accepting (O–H) atoms. **b**, Energy along the proton transfer reaction coordinate; note that the barrier height is higher than in **a** because it does not include ZPE. **c**, Change in the C–O distance and the distance between the centres of mass of the monomers along the proton transfer reaction minimum energy path on the computed two-dimensional PES, demonstrating the significant reorientation of the bases necessary to achieve a favourable alignment of the C–H–O moiety. **d**, Molecular orbitals at the initial (MIN), final (PT) and transition state (TS) structures of the lowest-energy 1,3-mU_2^+ conformer (with a circle marking the transferred proton) demonstrate the evolution of the wavefunction along the proton transfer pathway. Energies were computed with ωB97X-D/6-31 + G(d,p) and include ZPE correction.

hydrogen-bonded and π-stacked systems. In the former, the proton transfer reaction coordinate corresponds to a simple proton motion between the two uracil moieties due to an almost linear hydrogen bond ((N–H–O) = 177°) and a relatively short distance between the proton-accepting and proton-donating atoms (2.794 Å at the Franck–Condon geometry). Because of the collinear arrangement, elongation of one of the bonds (N–H) implies shortening of the other (O–H) bond, and no large changes are observed in other degrees of freedom (for example, relative orientation of the fragments) along the proton transfer reaction coordinate. Thus, proton transfer is essentially a one-dimensional process in these hydrogen-bonded systems.

In contrast, the structure of the stacked 1,3-mU_2 dimer is not optimal for proton transfer; that is, the C–O separation is 3.136 Å and (C–H–O) = 107° at the Franck–Condon relaxed geometry. Therefore, a considerable rearrangement of the bases along the proton transfer pathway is required to make the process energetically possible.

This is illustrated by the two-dimensional potential energy surface (PES) scan and the proton transfer reaction coordinates shown in Fig. 5a. Although one can imagine multiple reaction pathways on this excited potential energy surface, the lowest-energy proton transfer path involves a concerted change in the distances between the proton and the donating (C–H) and accepting (O–H) atoms. The transition state is nearly symmetric with respect to the C–H and O–H separation. In contrast to the hydrogen-bonded conformer, a simple elongation of the C–H bond does not correlate with O–H bond contraction, which requires reorientation of the bases. Thus, one-dimensional PES scans along either the C–H or O–H bonds (with all other degrees of freedom relaxed) result in a much higher proton transfer barrier. The complex character of the proton transfer reaction coordinate is illustrated by the changes in C–O separation and the distance between the centres of mass of the bases along the points corresponding to the minimal energy path on the two-dimensional surface (Fig. 5b). The C–O distance decreases by 0.6 Å as the system moves from the Franck–Condon relaxed structure to the transition state. The shallow (with respect to inter-fragment relative motion) shape of the potential energy surface determined by weak electrostatic and dispersion interactions in the ion allows for significant reorientation of the bases along the proton transfer coordinate necessary to achieve a favourable alignment of the C–H–O moiety. Near the transition state, the dimer assumes a T-shaped structure manifested by a large increase in the centre-of-mass separation shown in Fig. 5c. As the system passes over the transition state, it relaxes back to a stacked geometry.

The evolution of the electronic wavefunction along the proton transfer reaction coordinate is demonstrated by the shapes of the molecular orbitals (Fig. 5d) at the initial equilibrium (MIN), final (PT) and transition state (TS) structures. The initial hole is delocalized over both fragments, but in the transition state and proton transferred structures the unpaired electron is localized on the proton-donating base. Note that the shape of the molecular orbital in the proton transferred and transition state structures reveals hole delocalization over the C–H σ bonds. Therefore, the change in the electronic state character along the reaction path facilitates proton transfer by reducing the C–H bonding character and weakening the C–H bonds.

Although the complexity of the system does not allow all possible proton transfer pathways to be established as well as a quantitative prediction of the proton transfer rates, the experimental results unambiguously demonstrate that the proton transfer channel is very efficient in methylated species and that the reaction begins near the thermodynamic onset. By considering dimethyluracil as a model system of stacked base pairs, we demonstrate that ionization-induced proton transfer encounters only a moderate energy barrier (0.6 eV or 14 kcal mol^{-1}) due to the concerted reaction coordinate and complex evolution of the electronic wavefunction. We therefore speculate that protons may transfer along stacked ionized systems with no hydrogen bonds, or along non-conventional hydrogen bonds in various biological environments. For example, our observations suggest that methylation of DNA, which eliminates Watson–Crick hydrogen bonding, may not prevent excited/ionized-state proton transfer, which is known

to be important in photoexcitation- and oxidation-induced processes in DNA.

It is also possible that similar proton transfer mechanisms could be operational upon photoexcitation and ionization of plant biomass, which is made up of an intricate array of inter- and intra-molecular hydrogen-bonded as well as π-stacked networks[41,42]. The local electronic structure of stacked systems may have ramifications in a number of other fields. For instance, in scanning tunnelling microscopy and in other sensing techniques, hydrocarbons are detected on metal surfaces, where π-stacking is often involved. Proton transfer through these stacked systems could affect rates of reactions, which is important for catalysis studies[14].

Our results pave the way for more sophisticated experiments to directly probe the nature and dynamics of proton transfer in stacked systems and to investigate whether such novel proton transfer pathways are operational in realistic environments. Although the experiments and theory reported here are static in nature and do not interrogate the dynamics, they do provide the foundation and backdrop from which new experiments can be devised, and theory applied to interpret them. For instance, experiments using ultrafast VUV photons should allow direct mapping of proton transfer rates, and two-colour infrared–VUV spectroscopy should provide structural insight into the proton transfer mechanism. Inclusion of time-resolved pump–probe spectroscopy and molecular dynamics calculations would allow visualization of the actual proton transfer mechanism.

Methods

We used tunable synchrotron radiation and a variety of *ab initio* approaches following protocols used in previous studies[33,43] and described in detail in Supplementary Section S1. Briefly, the experiments were performed on a molecular beam apparatus coupled to a VUV monochromator on the Chemical Dynamics Beamline at the Advanced Light Source. A thermal vaporization source, an effusive or a supersonic molecular beam were used to introduce the bases into the gas phase. The bases and their dimers were ionized using photon energies between 8 eV and 11.5 eV and were detected using reflectron mass spectrometry. Deuterated 1,3-mU was synthesized (Supplementary Section S1) as it is unavailable commercially. Electronic structure calculations were performed using Q-CHEM[44] using methods ranging from EOM-IP-CCSD to density functional theory with a range of separated functionals and dispersion correction (wB97X-D).

Received 7 September 2011; accepted 7 February 2012; published online 18 March 2012

References

1. Schultz, T. *et al.* Efficient deactivation of a model base pair via excited-state hydrogen transfer. *Science* **306,** 1765–1768 (2004).
2. Ghosh, A. K. & Schuster, G. B. Role of the guanine N1 imino proton in the migration and reaction of radical cations in DNA oligomers. *J. Am. Chem. Soc.* **128,** 4172–4173 (2006).
3. Kennis, J. T. M. *et al.* Uncovering the hidden ground state of green fluorescent protein. *Proc. Natl Acad. Sci. USA* **101,** 17988–17993 (2004).
4. Mitchell, P. Coupling of phosphorylation to electron and hydrogen transfer by a chemi-osmotic type of mechanism. *Nature* **191,** 144–148 (1961).
5. Chakraborty, T. in *Charge Migration in DNA: Perspectives from Physics, Chemistry, and Biology* (Springer Verlag, 2007).
6. Decoursey, T. E. Voltage-gated proton channels and other proton transfer pathways. *Physiol. Rev.* **83,** 475–579 (2003).
7. Nagle, J. F. & Morowitz, H. J. Molecular mechanims for proton transport in membranes. *Proc. Natl Acad. Sci. USA* **75,** 298–302 (1978).
8. Marx, D., Tuckerman, M. E., Hutter, J. & Parrinello, M. The nature of the hydrated excess proton in water. *Nature* **397,** 601–604 (1999).
9. Sobolewski, A. L., Domcke, W. & Hattig, C. Tautomeric selectivity of the excited-state lifetime of guanine/cytosine base pairs: the role of electron-driven proton-transfer processes. *Proc. Natl Acad. Sci. USA* **102,** 17903–17906 (2005).
10. Perun, S., Sobolewski, A. L. & Domcke, W. Role of electron-driven proton-transfer processes in the excited-state deactivation adenine–thymine base pair. *J. Phys. Chem. A* **110,** 9031–9038 (2006).
11. Wahl, M. C. & Sundaralingam, M. C–H···O hydrogen bonding in biology. *Trends Biochem. Sci.* **22,** 97–102 (1997).
12. Marfurt, J. & Leumann, C. Evidence for C–H=O hydrogen bond assisted recognition of a pyrimidine base in the parallel DNA triple-helical motif. *Angew. Chem. Int. Ed.* **37,** 175–177 (1998).
13. Loganathan, D. & Aich, U. Observation of a unique pattern of bifurcated hydrogen bonds in the crystal structures of the *N*-glycoprotein linkage region models. *Glycobiology* **16,** 343–348 (2006).
14. Somorjai, G. A., Tao, F. & Butcher, D. in *Scanning Tunneling Microscopy in Surface Science* 189–217 (Wiley-VCH Verlag, 2010).
15. Keiluweit, M. & Kleber, M. Molecular-level interactions in soils and sediments: the role of aromatic π-systems. *Environ. Sci. Technol.* **43,** 3421–3429 (2009).
16. Crespo-Hernandez, C. E., Cohen, B., Hare, P. M. & Kohler, B. Ultrafast excited-state dynamics in nucleic acids. *Chem. Rev.* **104,** 1977–2019 (2004).
17. Middleton, C. T. *et al.* DNA excited-state dynamics: from single bases to the double helix. *Annu. Rev. Phys. Chem.* **60,** 217–239 (2009).
18. Kanvah, S. *et al.* Oxidation of DNA: damage to nucleobases. *Acc. Chem. Res.* **43,** 280–287 (2009).
19. Schreier, W. J. *et al.* Thymine dimerization in DNA is an ultrafast photoreaction. *Science* **315,** 625–629 (2007).
20. Bhosale, S. *et al.* Photoproduction of proton gradients with π-stacked fluorophore scaffolds in lipid bilayers. *Science* **313,** 84–86 (2006).
21. Sisson, A. L., Shah, M. R., Bhosale, S. & Matile, S. Synthetic ion channels and pores (2004–2005). *Chem. Soc. Rev.* **35,** 1269–1286 (2006).
22. Satzger, H., Townsend, D. & Stolow, A. Reassignment of the low lying cationic states in gas phase adenine and 9-methyl adenine. *Chem. Phys. Lett.* **430,** 144–148 (2006).
23. Meredith, P. & Sarna, T. The physical and chemical properties of eumelanin. *Pigment Cell Res.* **19,** 572–594 (2006).
24. d'Ischia, M., Napolitano, A., Pezzella, A., Meredith, P. & Sarna, T. Chemical and structural diversity in eumelanins: unexplored bio-optoelectronic materials. *Angew. Chem. Int. Ed.* **48,** 3914–3921 (2009).
25. Kobayashi, K. & Tagawa, S. Direct observation of guanine radical cation deprotonation in duplex DNA using pulse radiolysis. *J. Am. Chem. Soc.* **125,** 10213–10218 (2003).
26. Adhikary, A., Khanduri, D. & Sevilla, M. D. Direct observation of the hole protonation state and hole localization site in DNA-oligomers. *J. Am. Chem. Soc.* **131,** 8614–8619 (2009).
27. Gador, N. *et al.* Electronic structure of adenine and thymine base pairs studied by femtosecond electron-ion coincidence spectroscopy. *J. Phys. Chem. A* **111,** 11743–11749 (2007).
28. Nir, E., Plutzer, C., Kleinermanns, K. & de Vries, M. Properties of isolated DNA bases, base pairs and nucleosides examined by laser spectroscopy. *Eur. Phys. J. D* **20,** 317–329 (2002).
29. Plutzer, C., Hunig, I. & Kleinermanns, K. Pairing of the nucleobase adenine studied by IR–UV double-resonance spectroscopy and *ab initio* calculations. *Phys. Chem. Chem. Phys.* **5,** 1158–1163 (2003).
30. Zadorozhnaya, A. A. & Krylov, A. I. Ionization-induced structural changes in uracil dinners and their spectroscopic signatures. *J. Chem. Theoret. Comput.* **6,** 705–717 (2010).
31. Zadorozhnaya, A. A. & Krylov, A. I. Zooming into π-stacked manifolds of nucleobases: ionized states of dimethylated uracil dimers. *J. Phys. Chem. A* **114,** 2001–2009 (2010).
32. Golubeva, A. A. & Krylov, A. I. The effect of π-stacking and H-bonding on ionization energies of a nucleobase:uracil dimer cation. *Phys. Chem. Chem. Phys.* **11,** 1303–1311 (2009).
33. Bravaya, K. B., Kostko, O., Ahmed, M. & Krylov, A. I. The effect of π-stacking, H-bonding, and electrostatic interactions on the ionization energies of nucleic acid bases: adenine–adenine, thymine–thymine and adenine–thymine dimers. *Phys. Chem. Chem. Phys.* **12,** 2292–2307 (2010).
34. de Vries, M. S. & Hobza, P. Gas-phase spectroscopy of biomolecular building blocks. *Annu. Rev. Phys. Chem.* **58,** 585–612 (2007).
35. Munson, M. S. B. & Field, F. H. Chemical ionization mass spectrometry. I. General introduction. *J. Am. Chem. Soc.* **88,** 2621–2630 (1966).
36. Gronert, S., Feng, W. Y., Chew, F. & Wu, W. The gas phase acid/base properties of 1,3,-dimethyluracil, 1-methyl-2-pyridone, and 1-methyl-4-pyridone: relevance to the mechanism of orotidine-5′-monophosphate decarboxylase. *Int. J. Mass Spectrom.* **195–196,** 251–258 (2000).
37. Jochims, H. W., Schwell, M., Baumgartel, H. & Leach, S. Photoion mass spectrometry of adenine, thymine and uracil in the 6–22 eV photon energy range. *Chem. Phys.* **314,** 263–282 (2005).
38. Kabelac, M. & Hobza, P. At nonzero temperatures, stacked structures of methylated nucleic acid base pairs and microhydrated nonmethylated nucleic acid base pairs are favored over planar hydrogen-bonded structures: a molecular dynamics simulations study. *Chem. Euro. J.* **7,** 2067–2074 (2001).
39. Kabelac, M. & Hobza, P. Potential energy and free energy surfaces of all ten canonical and methylated nucleic acid base pairs: molecular dynamics and quantum chemical *ab initio* studies. *J. Phys. Chem. B* **105,** 5804–5817 (2001).
40. He, Y. G., Wu, C. Y. & Kong, W. Photophysics of methyl-substituted uracils and thymines and their water complexes in the gas phase. *J. Phys. Chem. A* **108,** 943–949 (2004).

41. Boerjan, W., Ralph, J. & Baucher, M. Lignin biosynthesis. *Ann. Rev. Plant Biol.* **54,** 519–546 (2003).
42. Takahashi, L. K. *et al.* VUV photoionization and mass spectrometric characterization of the lignin monomers coniferyl and sinapyl alcohol. *J. Phys. Chem. A* **115,** 3279–3290 (2011).
43. Belau, L., Wilson, K. R., Leone, S. R. & Ahmed, M. Vacuum–ultraviolet photoionization studies of the microhydration of DNA bases (guanine, cytosine, adenine, and thymine). *J. Phys. Chem. A* **111,** 7562–7568 (2007).
44. Shao, Y. *et al.* Advances in methods and algorithms in a modern quantum chemistry program package. *Phys. Chem. Chem. Phys.* **8,** 3172–3191 (2006).

Acknowledgements

Experiments were carried out at the Advanced Light Source, and the d6-1,3-mU was synthesized at the Molecular Foundry, both at Lawrence Berkeley National Laboratory. Berkeley participants are supported by the Office of Science, Office of Basic Energy Sciences, of the US Department of Energy (contract no. DE-AC02-05CH11231), through the Chemical Sciences Division (A.G., O.K., S.R.L., M.A.) and the Materials Sciences Division (R.K.). R.K. is also supported by the Defense Threat Reduction Agency (IACRO-B0845281). This work was conducted in the framework of the *iOpenShell* Center (iopenshell.usc.edu), supported by the National Science Foundation through CRIF:CRF (CHE-0625419 + 0624602 + 0625237 and CHE-0951634, to A.I.K.) grants.

Author contributions

M.A. conceived and designed the experiments. A.G. and O.K. conducted the experiments. R.K. synthesized the deuterated compounds. K.B.B. and A.I.K. performed electronic structure calculations. A.G. and K.B.B. contributed equally to this work. A.G., K.B.B., A.I.K., M.A. and S.R.L. co-wrote the paper.

Additional information

The authors declare no competing financial interests. Supplementary information accompanies this paper at www.nature.com/naturechemistry. Reprints and permission information is available online at http://www.nature.com/reprints. Correspondence and requests for materials should be addressed to A.I.K. and M.A.